Xin Dou
Department of Mechanical and Aerospace Engineering, University of Missouri, Columbia, MO 65211

Yijin Mao
Department of Mechanical and Aerospace Engineering, University of Missouri, Columbia, MO 65211

Yuwen Zhang[1]
Department of Mechanical and Aerospace Engineering, University of Missouri, Columbia, MO 65211
e-mail: zhangyu@missouri.edu

Effects of Contact Force Model and Size Distribution on Microsized Granular Packing

Granular packing of microsized particles with different size distributions and contact force models is studied using discrete element method (DEM). Three kinds of size distributions, monosized, uniform, and Gaussian, with mean diameter of 50, 60, and 70 μm are studied. Two aspects of microscale particle packing issues are addressed: one is the importance of van der Waals force when the particle size approaching to microscale, the other one is the structure variation caused by different contact force models. The results indicate that compared with contact force, the van der Waals force contributes very insignificantly to the final packing structure. The packing structures obtained using two different force models are similar to each other. The effects of particle size and its distribution on the packing structure are more significant than the force model.
[DOI: 10.1115/1.4025969]

Keywords: additive manufacturing, distinct element method, size distribution, granular matter

Introduction

Particle packing has been studied experimentally and numerically in the recent years due to its wide applications in physics and engineering. Mechanical phenomena and physical properties in granular materials, such as fluid flow, stress distribution, and electrical conductivity [1], and modeling the structure of materials such as liquids, amorphous, and ceramic materials [2], have been studied. Generally speaking, packing is a dynamic process that involves different kinds of forces. These forces control and determine the packing dynamics and properties during the packing process. In order to illustrate the model clearly and facilitate computation, the forces that affect the packing structures can be divided into two main groups: one is contact force that includes the normal and tangential contact forces, and the other group is conservative forces that include the gravity and van der Waals force. The viscoelastic and frictional forces that are generated when particles collide with each other are considered to be contact force.

Researchers have experienced difficulty in generating the structural information that can fully match what they measured experimentally [3]. Fortunately, recent works in this area demonstrated that this kind of problems can be solved using the DEM [4–8]. On the other hand, algorithms are also important for simulation process. Gan et al. predicted the packing structure of particles with arbitrary shapes and sizes accurately [9]. They avoided many difficulties and unnecessary problems encountered by the conventional algorithms when dealing with nonspherical particles packing. Some early simulation algorithms were based on kinematics and did not consider packing as a dynamic process [10–12]. Recently, the roles of interparticle forces have been recognized, and the approaches of taking the interparticle forces into account properly have been developed. In order to simulate the final packing result more appropriately, many models to calculate the interaction among particles have been proposed [13–17]. However, it has been known for years that the final packing structure of particles is dominated by factors such as packing method, material properties, and particle size and associated distributions. Many existing efforts in the literature focused on the simulation of monosized particles packing [18–20]. Jia et al. studied granular packing of spherical particles with different sizes distributions using DEM [21–23]. Besides different sizes and distributions, van der Waals force, which is simply ignored in most of contact models, is accounted for in Ref. [23] as the size of particle approaches to microscale. At the millimeter-scale, van der Waals force is negligible, but at the micrometer scale van der Waals force cannot be simply ignored under the similar situation [24–27].

In this paper, the DEM will be employed to study the packing structure of micrometer-scale particles with different sizes (50, 60, and 70 μm). Three different kinds of distributions (monosized, uniform, and Gaussian) will be studied. The objective of this work is to identify a more accurate and efficient model for simulation of microscale granular packing and to reveal the role of the van der Waals force in microsized packing. LIGGGHTS [28] that is based on LAMMPS [29], aiming to solving particle related problem in industrial applications, is used to simulate the packing process. By comparing the simulated and associated packing results, the validity of the approach can be examined. The resulting packing structures are analyzed in terms of packing density, coordinate number, and radial distribution function (RDF) and force distribution, respectively.

Physical Models and Methods

The motions of particles can be divided into two parts: translation and rotation. Translational motion that is movement changing the position of the particles is described using the Newton's second law

$$m_i \frac{d^2\mathbf{X}_i}{dt^2} = \mathbf{F}_i \tag{1}$$

where m_i is the mass of the ith particle, and $\mathbf{X}_i$ is the position of the ith particle. The particle motion can be caused by three kinds of forces: contact force, van der Waals force, and gravity. The gravity is a kind of conservative force and is easy to calculate compared with the other two kinds of forces. When the two particles collide to each other, the contact force acting on the particles can be decomposed into normal and tangential components.

[1]Corresponding author.
Manuscript received May 31, 2013; final manuscript received November 1, 2013; published online January 3, 2014. Assoc. Editor: Yong Huang.

According to the nonlinear Hertz theory [30], the normal contact force acting on the particle i by the particle j can be expressed as

$$\mathbf{F}^n = \left(K_n\delta_n - \frac{3}{2}\gamma K_n\left(\mathbf{v}_{ij}\cdot\mathbf{n}_{ij}\right)\right)\mathbf{n}_{ij} \tag{2}$$

where the effective stiffness K_n is defined as

$$K_n = \frac{4}{3}Y^*\sqrt{R^*\delta_n} \tag{3}$$

where $\mathbf{v}_{ij}$ is the velocity of particle i relative to the velocity of particle j, $R^* = R_iR_j/(R_i+R_j)$ is the effective radius that is the geometric mean of R_i and R_j, $\delta_n = (R_i+R_j) - |\mathbf{D}_{ij}|$ is the overlap in normal direction, where $\mathbf{D}_{ij}$ represents the distance between the spherical centers of particle i and particle j, and $Y^* = Y/[2(1-\sigma_P^2)]$ is defined in terms of Young's modulus Y of particles and Poisson ratio σ_P of the materials from which the particle are made. In Eq. (2), γ is the damping coefficient, and $\mathbf{n}_{ij}$ is unit vector connecting jth and ith particles.

In addition, the tangential displacement should be obtained before calculating the tangential force. Different means of calculating overlaps lead to different tangential contact force models. Tangential displacement generated by deformations of particles, which varies with time in the packing process, is determined as

$$\xi_t = \int_{t_0}\mathbf{v}_t dt \tag{4}$$

$$\xi_{\max} = \mu_s\frac{2-\sigma_P}{2-2\sigma_P}\delta_n \tag{5}$$

$$\mathbf{v}_t = \left[\left(\mathbf{v}_i - \mathbf{v}_j\right)\cdot\mathbf{t}_{ij}\right]\mathbf{t}_{ij} + \left(\boldsymbol{\omega}_i + \boldsymbol{\omega}_j\right)\times\mathbf{R}_{ij} \tag{6}$$

where $\boldsymbol{v}_t$ is the tangential relative velocity, t_0 is the time when the two particles just collide with each other without deformation, and μ_s is the sliding friction coefficient. If the tangential displacement reaches to a certain value, sliding friction will occur between the two particles. In order to differentiate from sliding friction effect, the maximum value for tangential displacement that is represented by parameter $\xi_{\max}$ is defined. The value of $\xi_{\max}$ is determined by the deformation calculated in normal direction, Poisson ratio σ_P and sliding friction coefficient μ_s. Last but not the least, $\boldsymbol{\omega}$ represents the angular velocity of particles and $\boldsymbol{t_{ij}}$ is unit vector that is perpendicular to normal direction and parallel to the direction of relative velocity between the ith particle and jth particle. Mathematically, it should satisfies $\mathbf{t}_{ij}\cdot\mathbf{n}_{ij} = 0$ and $\mathbf{t}_{ij}\times\mathrm{v}_{ij} = 0$. It is worth to mention that $\boldsymbol{t_{ij}}$ is opposite to the direction of deformation, and independent of the direction of velocity. It is very important to determine unit tangential vector in order to further calculate the tangential force.

Once tangential displacement is obtained, the tangential force can be obtained based on the Mindlin-Deresiewicz theory [31–33]

$$\mathbf{F}^t = \mu_s|\mathbf{F}^n|\left(1 - \frac{|\xi_t|}{\xi_{\max}}\right)\frac{\xi_t}{|\xi_t|} \tag{7}$$

where $|\mathbf{F}^n|$ is the magnitude of the contact force in the normal direction, and $\boldsymbol{\xi}_t$ is the tangential displacement calculated in Eq. (4).

Since the size of the particle cannot be ignored, the rotational motion has to be described through analogy to Newton's 2nd law of motion

$$I_i\frac{d^2\theta_i}{dt^2} = \mathbf{T}_i \tag{8}$$

where I_i is the moment of inertia that is a property of a distribution of mass in space that measures its resistance to rotational acceleration about an axis, and I_i equals to $0.4m_iR_i^2$ here. The angle of particle i is represented by $\boldsymbol{\theta}_i$.

The torque generated by rolling friction is given by

$$\mathbf{T}_{ij}^r = -\mu_r R_i|\mathbf{F}_{ij}^n|\boldsymbol{\omega}_i \tag{9}$$

where μ_r is rolling friction coefficient, and the torque caused by tangential force is determined by

$$\mathbf{T}_{ij}^t = \mathbf{R}_i\times\mathbf{F}_{ij}^t \tag{10}$$

The van der Waals force can be calculated using the following formula [34]:

$$\mathbf{F}_v = -\frac{\mathrm{Ha}}{6}\frac{64R_i^3R_j^3\left(h+R_i+R_j\right)}{\left(h^2+2R_ih+2R_jh\right)\left(h^2+2R_ih+2R_jh+4R_iR_j\right)}\mathbf{n}_{ij} \tag{11}$$

$$h = |\mathbf{D}_{ij}| - \left(R_i+R_j\right) \tag{12}$$

where Ha is the Hamaker constant that is determined by the properties of material, and h is the distance between surfaces of two interactional particles (distance between the centers of two the particles minus the sum of the radii). It should be pointed out that a minimum value $h_{\min}$ for h is chosen in order to prevent numerical instability. In other words, if h is smaller than $h_{\min}$, h is forced to be equal to $h_{\min}$ ($h_{\min} = 10$ nm in this work).

The open-source software LIGGGHTS is designed to simulate large-sized particles packing process where the van der Waals force can be ignored. It has a number of particle contact models, among which Hertz History model [35–37] has been cited by many researchers and is chosen as a representative of macroscale packing model to be compared with the present model.

Different from contact model of microscale collision, only normal force and tangential force are considered in Hertz History model. The normal contact force of Hertz History model is given as

$$\mathbf{F}^n = \left(K_n\delta_n - \gamma_n\mathbf{v}\cdot\mathbf{n}_{ij}\right)\mathbf{n}_{ij} \tag{13}$$

where $K_n = \frac{4}{3}Y^*\sqrt{R^*\delta_n}$, $\gamma_n = -2\sqrt{\frac{5}{6}}\beta\sqrt{S_nm^*}$, $\beta = \frac{ln(e)}{\sqrt{ln^2(e)+\pi^2}}$, $S_n = 2Y^*\sqrt{R^*\delta_n}$, $m^* = m/2$, and e is the coefficient of restitution. Compared to normal contact force in the present model (see Eq. (2)), the first term that is related to the overlap in the normal direction is identical. It is different from present model, however, that the Hertz History model considers damping coefficient as a variable that depends on the mass of the particles, the coefficient of restitution, Young's modulus and normal direction overlap.

The tangential force of Hertz History model is calculated through

$$\mathbf{F}^t = \left(K_t|\xi_t| - \gamma_t\mathbf{v}\cdot\mathbf{t}_{ij}\right)\frac{\xi_t}{|\xi_t|} \tag{14}$$

where $K_t = 8G^*\sqrt{R^*\delta_n}$, $\gamma_t = -2\sqrt{\frac{5}{6}}\beta\sqrt{S_tm^*}$, $G^* = ((Y/4(2+\sigma)(1-\sigma))$, $S_t = 8G^*\sqrt{R^*\delta_n}$, and $m^* = m/2$.

The simulation region is a hexahedron, whose six boundary faces are considered as elastic walls that share material properties with particles in the box. The initial volume fraction of particles in the simulation box is kept the same for all cases. As a result, the simulation region will be larger to ensure there is enough space to keep these particles when larger particles pour into the box. In other words, the length, width, and the height of the simulation box will vary with the size of particle and increase with the same rate, which is based on the particle sizes. For monosized particles, for example, the minimum size of this box is 1.0 mm × 1.0 mm × 1.2 mm, while the maximum size is 1.4 mm × 1.4 mm × 1.54 mm. In the beginning, there are 4500 particles distributed randomly in the entire region, but no particle gets in touch with other particles or boundaries. The time step must be sufficiently small to avoid unrealistically large deformation of particles when colliding with other particles or walls in the DEM

Table 1 Values of parameters used in simulation process

Parameters	Values
Particle density, ρ	2504 kg/m^3
Hamaker constant, Ha	6.5×10^{-20} J
Young's modulus, Y	10^7 N/m^2
Restitution coefficient, e	0.95
Sliding friction coefficient, μ_s	0.3
Rolling friction coefficient, μ_r	2×10^{-3}
Damping coefficient, γ	2×10^{-5} s
Poison ratio, σ_P	0.3

simulations. The unrealistically large deformation will lead to meaningless unrealistic contact force. The time step-independence test for packing simulation indicated that a time step of 2×10^{-7} s is sufficient to obtain consistent and accurate results. The comparison will be more meaningful and persuasive when all cases have the same time step.

RDF, which is also called pair correlation function or pair distribution function, is an important function to characterize the packing structure. It describes how number density changes as a function of distance from a reference particle or the probability to find a particle in a shell dr at the distance r of another particle chosen as the reference point

$$g(r) = \frac{V}{N} \frac{dN(r)}{4\pi r^2 dr} \tag{15}$$

where V represents the total volume of the hexahedron that all particle occupy, N is the total number of particles, and $dN(r)$ is the number of particles in a shell of width dr at distance r from the reference particle.

Since the purpose of this work is to study the variation caused by size distribution and contact force model, all the particles are adapted with the same material [23] whose properties are shown in Table 1. The size distributions chosen include monosized, uniform, and Gaussian. And the mean diameters for each distribution vary in 50 μm, 60 μm, and 70 μm, respectively. In the entire simulation process, the RDF results and force distributions are recorded from the beginning of the simulation process. The results of final packing structure will be recorded when all the particles turn to be static equilibrium, which means that the RDF function does not change anymore even the simulation is proceeded.

Results and Discussions

Eighteen cases with the same number of particles, three types of particle sizes and distributions, and two kinds of contact force models are simulated. All the parameters shown in the figures are nondimensional variables. Three basic characteristic values are chosen to do the nondimensionalization: length L mass M and energy E whose values are 5.0×10^{-5} m, 1.0×10^{-10}kg, and 1.0×10^{-12} J, respectively. The numbers that appeared in the figures are all nondimensional values and if multiplied by the characteristic values mentioned previously, the real values can be easily obtained. The porosities and coordination numbers are calculated in order to characterize the final packing structure. Even particles' deformation is considered and calculated to obtain more accurate contact force but in the entire packing process all the particles are still considered to be rigid body. If the distance between the centers of two particles is less than a critical distance, $1.01(d_1 + d_2)/2$,

Table 2 Porosity and coordination number for present model

	Porosity			Coordination number		
Diameter	Monosized	Uniform	Gaussian	Monosized	Uniform	Gaussian
50 μm	0.395	0.392	0.329	6.25	6.29	6.34
60 μm	0.398	0.388	0.378	6.15	6.28	6.25
70 μm	0.416	0.354	0.316	6.21	6.31	6.26

Table 3 Porosity and coordination number for Hertz History model

	Porosity			Coordination number		
Diameter	Monosized	Uniform	Gaussian	Monosized	Uniform	Gaussian
50 μm	0.384	0.365	0.345	6.61	6.72	6.74
60 μm	0.392	0.322	0.319	6.75	6.68	6.69
70 μm	0.394	0.353	0.382	6.58	6.76	6.77

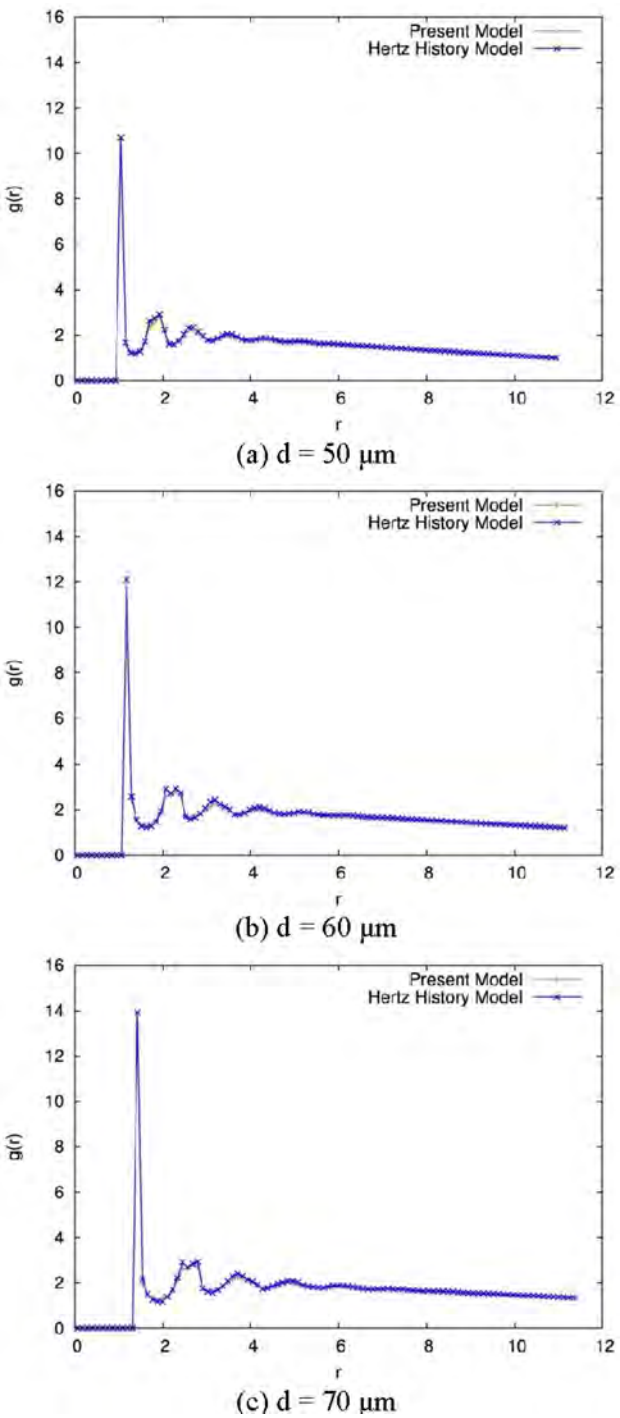

Fig. 1 RDF for monosized particles

where d_1 and d_2 are the two particles' diameters, the two particles are considered to be in direct contact [23]. Tables 2 and 3 show that when the diameters of particles that have the same distribution increase, the coordination number and porosity are independent of particle size which is consistent with the work done by Brilliantov et al. [35]. However, when the particles with the same size but different distributions are focused, the results are quite clear. It can be found that particles with uniform and Gaussian distributions have larger coordination number and lower porosity compared with that of the monosized particles. This result can be explained as even the mean diameter is the same but when smaller and larger particles are mixed, they will have more opportunity to contact with others and pack more densely.

Figure 1 shows comparison of RDF between present model and Hertz History model for monosized particles packing cases ($d = 50$–$70\ \mu$m). It can be observed that there are three primary peaks with a decreasing trend on the curve shown in Fig. 1(*a*). The first peak reaches to 10.699 when r equals to 1.045, which hints that all the particles are well packed and averaged distance between particles is close to the diameter of the particles. The second and third peaks reach to 2.913 and 2.358 at r equals to 1.925 and 2.695, respectively. Figures 1(*b*) and 1(*c*) show similar phenomena and demonstrate RDF variation with the particles diameter as well. In Fig. 1(*b*), the first peak reaches to 12.096 when r equals to 1.176; while the second and third peaks reach to 2.920 and 2.437 when r equals to 2.296 and 3.192, respectively.

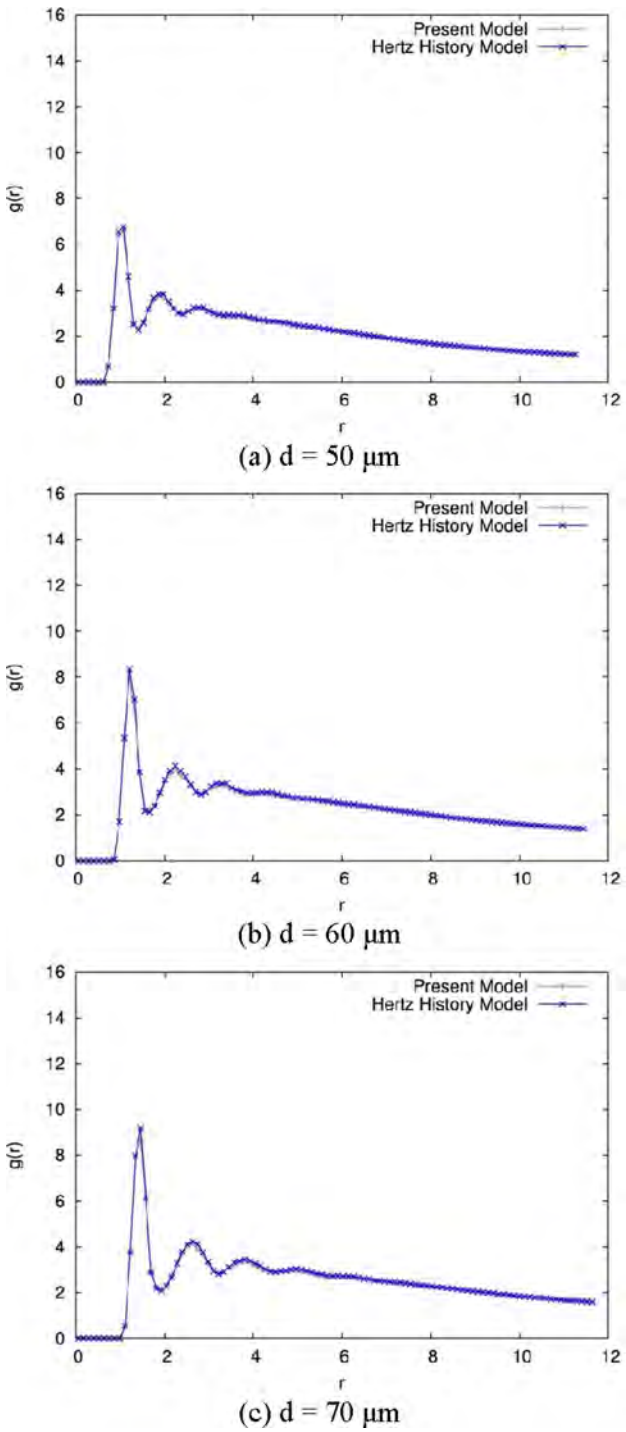

Fig. 2 RDF for uniform distribution particles

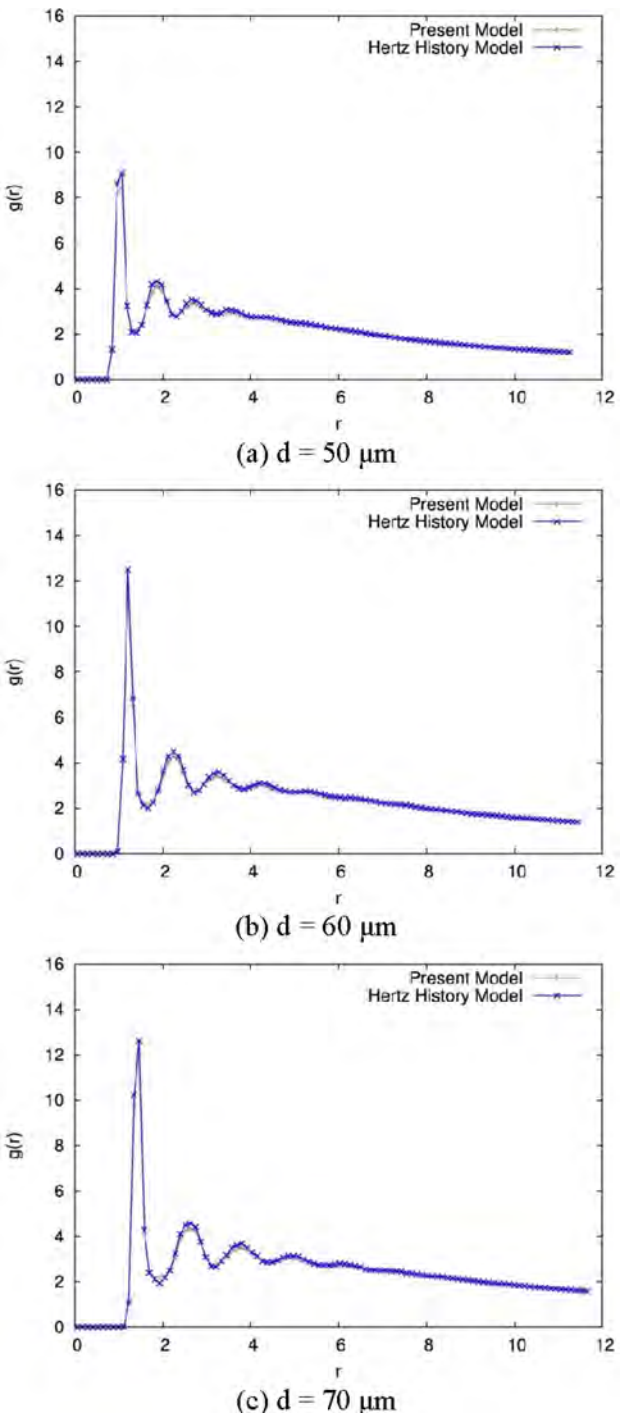

Fig. 3 RDF for Gaussian distribution particles

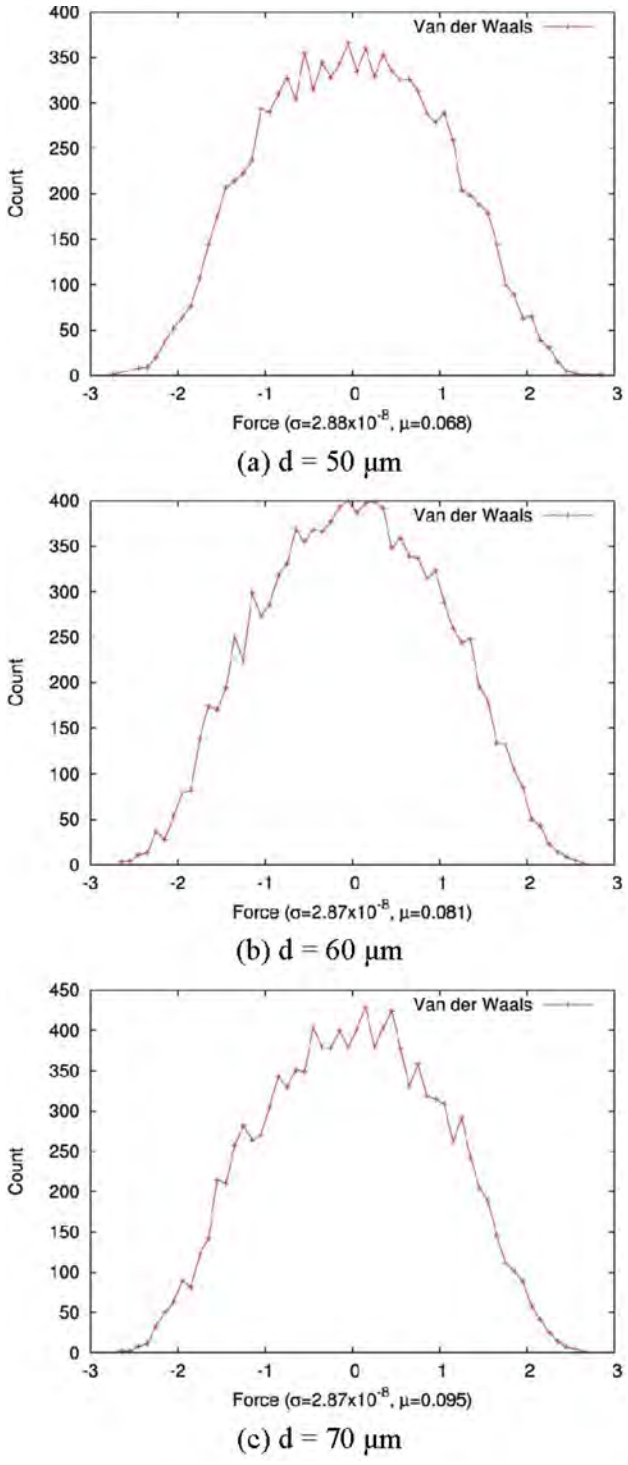

Fig. 4 Van der Waals force distribution for monosized particles

Similarly, the first peak reaches to 13.935 when r equals to 1.425 in Fig. 1(*c*), while the second and third reaches to 2.908 and 2.340 when r equals to 2.451 and 3.705, respectively. It can be found for all three diameters that the curves of both force models are very similar to each other. The location of peak values slightly moves to right with increasing particle diameter. This phenomenon demonstrates that the larger the particle diameter is, the more loosely the particles will pack.

Figure 2 shows the RDF when the particle sizes satisfy the uniform distribution, and the diameter difference between the nearest particles is 1 μm. For the case that mean diameter equals to 50 μm, particle diameters are from 35 to 65 μm. When particles' mean diameter reaches to 60 μm, the particle diameters uniformly vary from 45 μm to 75 μm. Finally, particles' diameters uniformly vary from 55 μm to 85 μm in order to obtain a mean diameter of 70 μm. It is necessary to point out that for uniform distribution the number of particles with each size in the range is identical. For example, in the case that the particle mean diameter equals to 50 μm, the number of particles having diameter from 35 μm to 65 μm (with 1 μm increment) are identical. Similarly to the phenomena indicated in Fig. 1, the shapes of RDF have similar trends. However, the first peak values are quite different due to the variation

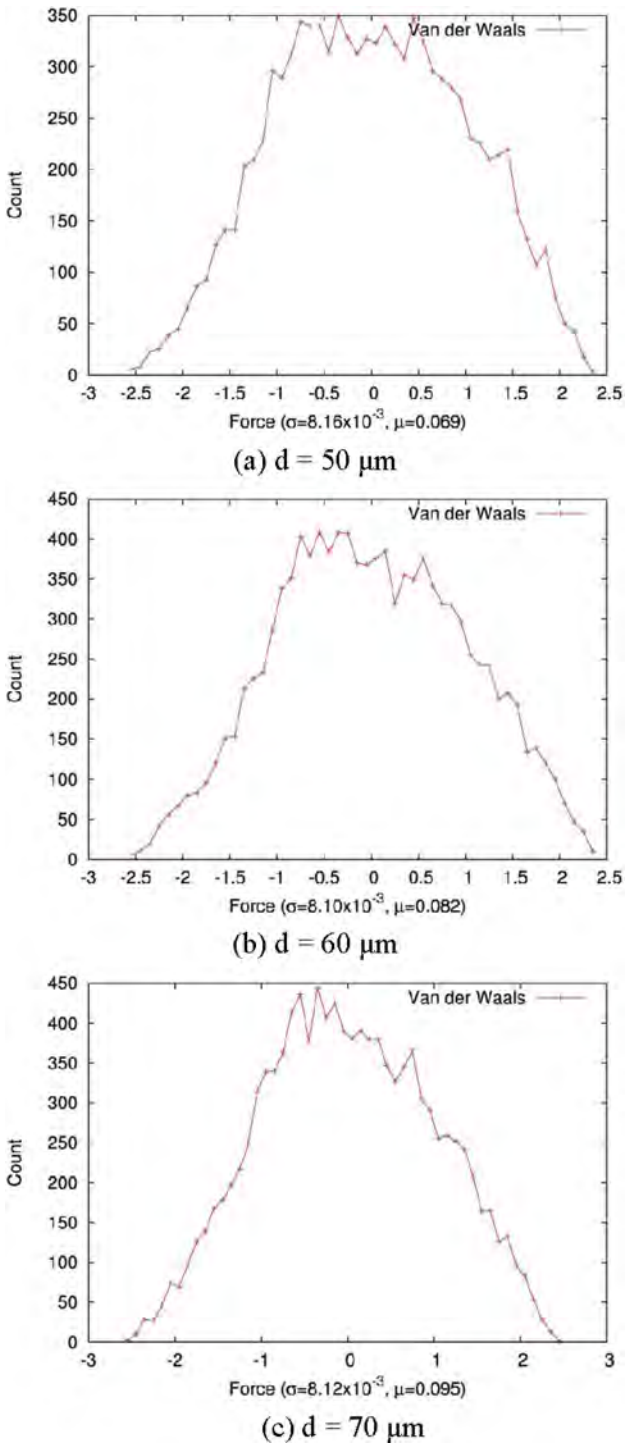

Fig. 5 Van der Waals force distribution for uniform distribution particles

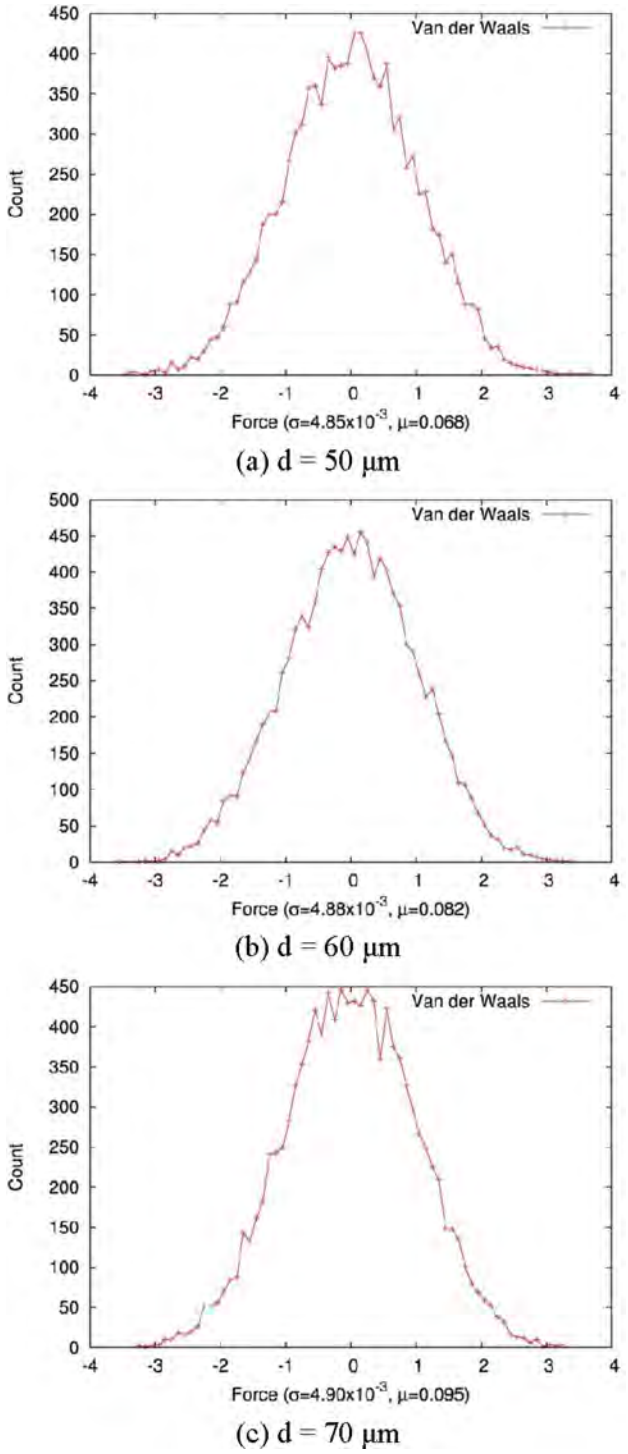

Fig. 6 Van der Waals force distribution Gaussian distribution particles

of size distribution. For example, the first peak value is around 6 for uniform distribution as shown in Fig. 2. Also, it is easy to draw a conclusion that when the final packing structure is desired, two contact models have similar packing structure based on these RDF responses after observing and comparing the plots.

Figure 3 demonstrates the RDF results for the system of particles with Gaussian size distribution. The standard deviation, σ_S, is set as 15 μm for all three sizes. It can be observed that when particles' diameters increase, the first peak will appear at larger r value which means that even when particles have the same deviation, change of diameters still contribute significantly to the packing results.

Figures 4–6 demonstrate the standard deviation represented by σ_S and the mean value of force magnitude represented by μ of the van der Waals force distribution. Both of them are nondimensional variables which can be converted to real value by multiplying characteristic value described previously. Figure 4 illustrates the van der Waals force distribution of monosized packing for different particle diameters. It can be found that the dimensionless average Van der Waals force, μ, increases as the diameter increases because the large particle diameter leads to large van der Waals force according to Eq. (11).

Figure 5 shows the magnitude of van der Waals force distribution for packing of particles with uniform size distributions. It can

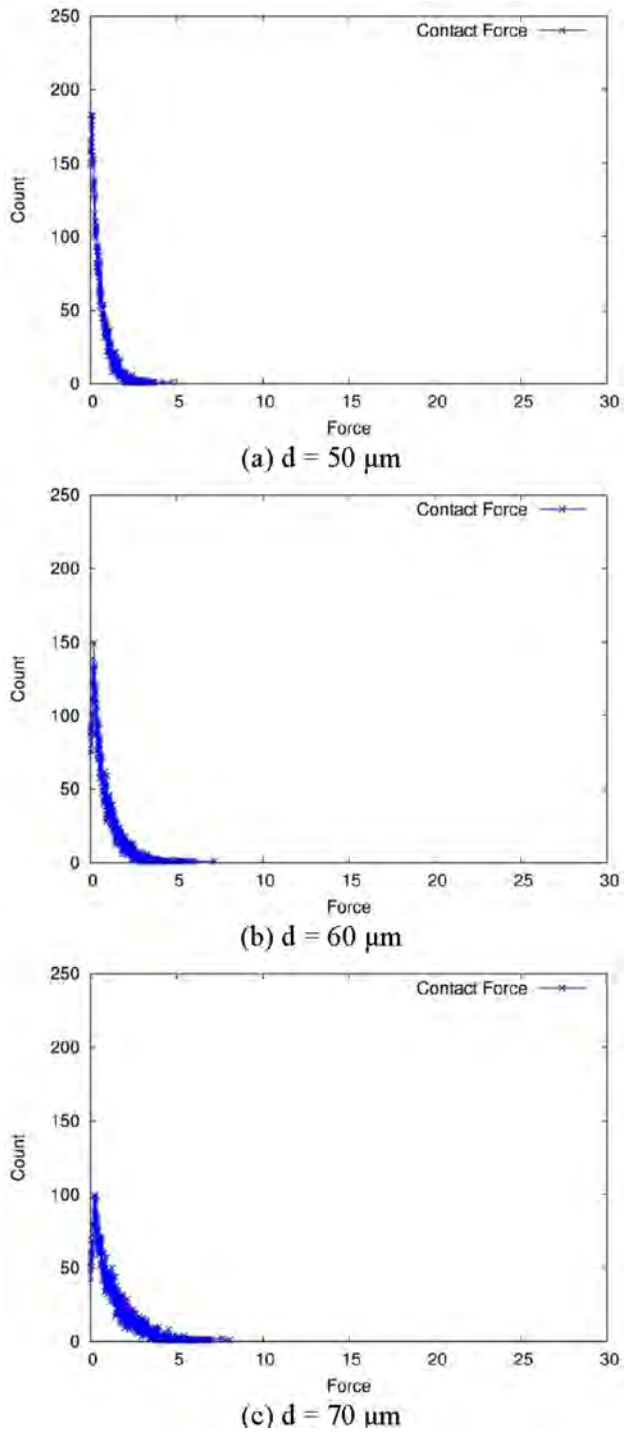

Fig. 7 Contact force distribution for monosized particles

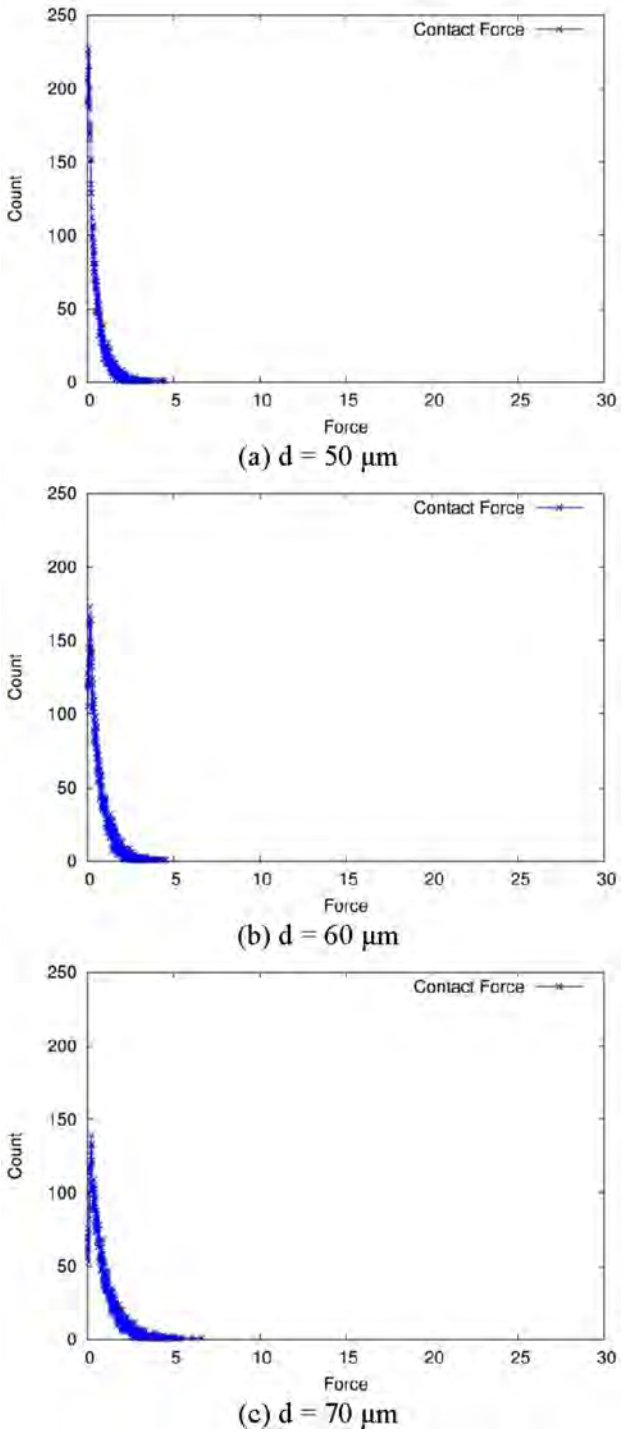

Fig. 8 Contact force distribution for uniform distribution particles

be found that the Van der Waals force distribution is similar in counts compared with that in Fig. 4 and the magnitude of van der Waals force that represented by μ value is almost the same as those in monosized cases when the particles have the same mean diameter. This phenomenon indicates that particle diameter mainly effect the van der Waals force magnitude.

Figure 6 presents the effect of van der Waals to particle packing with Gaussian distribution. The results show that the magnitudes of van der Waals force of particles that have the same mean diameter are very similar to each other even when their distributions are totally different. It also demonstrates that similar to the RDF results which are mainly affected by particle diameters, the magnitude and counts of van der Waals force are also dominated by the particle size.

The force distributions for contact forces for three different size distributions are shown in Figs. 7–9. It has to be mentioned that gravity is important driving force for particle packing so that particles will pack with each other at the bottom of the simulation box at the end. But in Figs. 7–9, the gravity is not presented and the curves represent the nondimensional value for contact forces only. The reason that gravity is not included contains two parts: one is that the magnitude of gravity is much larger than that of contact force, and if it is added into the plots the real magnitude

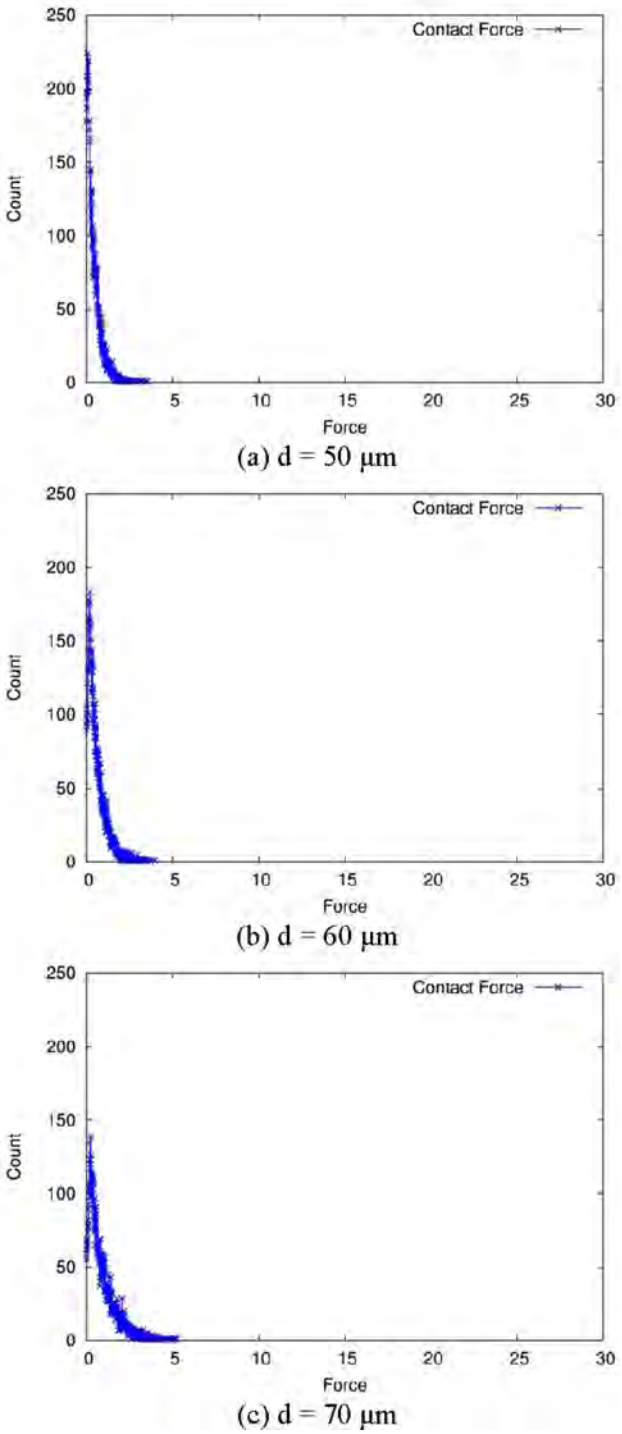

Fig. 9 Contact force distribution for Gaussian distribution particles

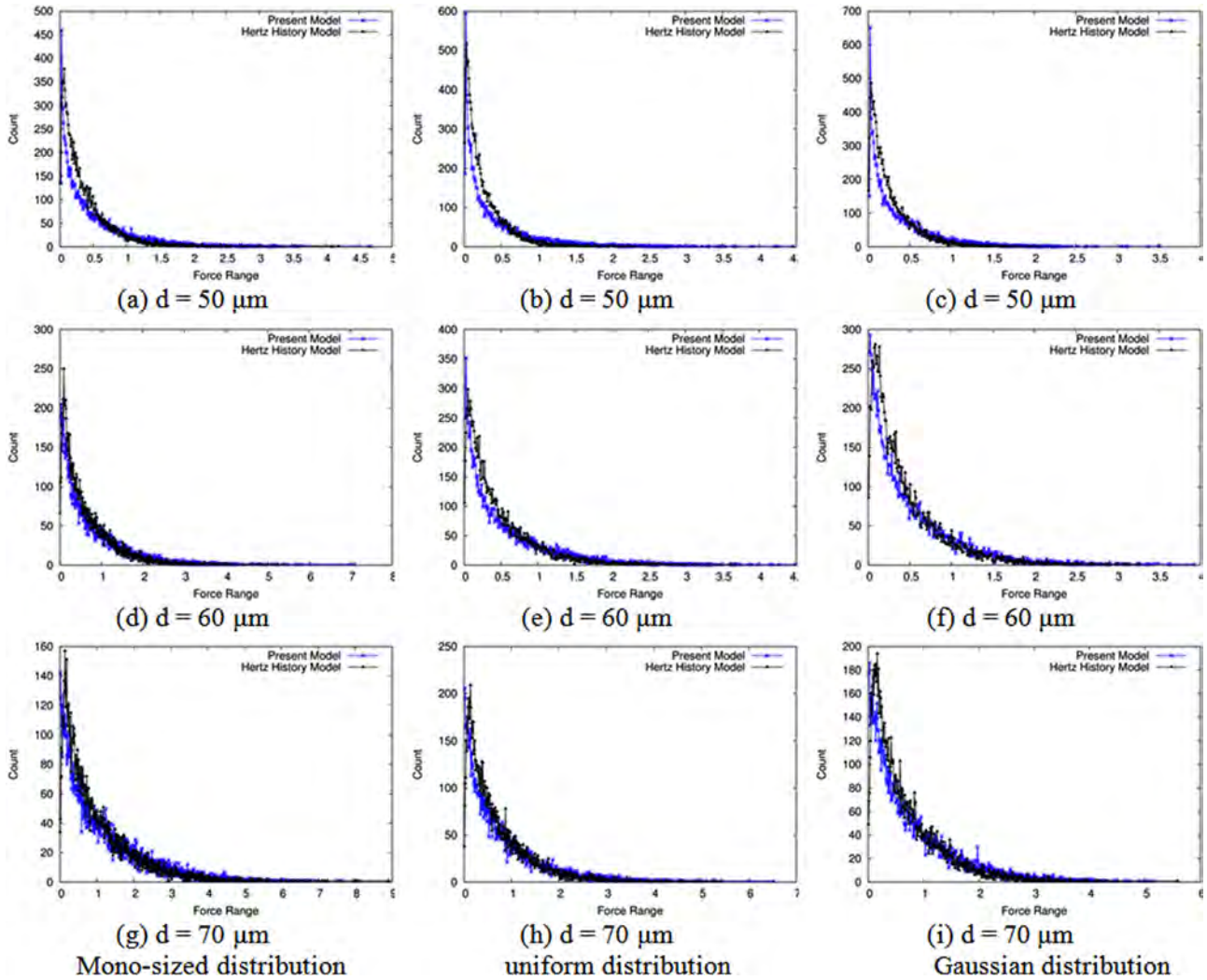

Fig. 10 Resultant force distributions

and tendency of contact forces will not be observed clearly; the other reason is that the acting point of contact force and that of gravity are different. Physically, gravity acts on the mass centers of particles while contact force exerts on the contact point generated by two contacting particles. It can be seen from Fig. 7 that the average of contact forces increases as the particle diameter increases for monosized packing. For most of contact models, calculation of deformation of colliding particles is a necessary procedure to obtain contact force. The deformation term is so important that it appears in every formula that aims to calculate contact force in which the overlaps contribute significantly to the deformation of particles.

Figure 8 presents the contact forces for packing of particles with uniform size distribution. It can be observed that when mean diameter of particles increases, the magnitude of contact forces increases. In other words, larger mean diameter particles with the same distribution will produce larger contact forces. Similar conclusion can be obtained from Fig. 9 which shows the contact forces for particles with Gaussian distribution. But compared with the result for monosized and uniform distribution particle packing, the magnitude of contact forces for this case is slightly smaller. This is mainly because when two particles with different sizes contacted with each other, the overlap produced is less than that generated by two particles with the same size.

There are many kinds of forces that affect the packing process and the two kinds of forces are discussed above: van der Waals force and contact force. Since Hertz History model does not consider van der Waals force, its resultant force is equal to the contact force in the following analysis. Based on the results from Figs. 4–9, van der Waals force, and contact force increase with increasing particle diameter. Figure 10 shows the resultant force distribution for different size distributions. It reveals that the effects of particle size and its distribution are more significant than the contact force model.

In the aspect of force magnitude, the distributed magnitude of contact forces is much larger than that of van der Waals forces. No matter what the diameter is or what the distribution is the contact forces probability distributions show exponential-like tail while the distribution of van der Waals forces is like a bell-shape. It is found that the resultant force of Hertz History model is slightly larger than that of the present model. Besides, two curves in each RDF result are very similar to each other. When particles have the same diameter and distribution the final packing structures are very alike even when the present model considers van der Waals force while the other does not.

Conclusions

Granular packing of particles with three different sizes and three different size distributions (monosized, uniform, and Gaussian) are simulated using discrete element method. In addition to the contact force, four kinds of forces are considered in the simulations which include two dissipative forces: viscoelastic and frictional force, and two conservative forces: gravity and van der

Waals force. The effect of van der Waals force on the packing structure of particles in micrometer domain has been systematically investigated. The results showed that the effect of van der Waals force is not significant for the particle size and its distributions investigated in this paper. It is also found that even though our model is much simpler than the Hertz History model, the final packing structure is very similar. Moreover, the tendencies of the force distributions and RDF results are similar when particles have the same diameter and distribution. The effects of particle size and its distribution are more significant than the force model.

Acknowledgment

Support for this work by the U.S. National Science Foundation under grant number CBET-1066917 is gratefully acknowledged.

Nomenclature

e = coefficient of restitution
g = gravity, m/s^2
h = distance between the centers of two particles minus the sum of their radius, m
Ha = Hamaker constant, J
m = mass of particle, kg
R = radius of particle, m
v = velocity, m/s
Y = Young's modulus, Pa

Greek Symbols

γ = damping coefficient, s
δ = overlap, m
ξ = tangential displacement, m
μ = mean value of van der Waals force
μ_s = sliding friction coefficient
μ_r = rolling friction coefficient
σ = deviation for van der Waals force
σ_S = standard deviation
σ_P = Poisson ratio
ω = angular velocity, rad/s

References

[1] German, R. M., 1989, *Particle Packing Characteristics*, Metal Powder Industries Federation, Princeton, NJ.
[2] Finney, J. L., 1970, "Random Packings and the Structure of Simple Liquids. I. The Geometry of Random Close Packing," Proc. R. Soc. London, Ser. A, **319**, pp. 479–493.
[3] Clarke, A. S., and Wiley, J. D., 1987, "Numerical Simulation of the Dense Random Packing of a Binary Mixture of Hard Spheres: Amorphous Metal," Phys. Rev. B, **35**, pp. 7350–7356.
[4] Owen, D. R. J., Feng, Y. T., Neto, E. A. D. S., Cottrell, M. G., Wang, F., Pires, F. M. A., and Yu, J., 2004, "The Modeling of Multi-Fracturing Solids and Particulate Media," Int. J. Numer. Methods Eng., **60**, pp. 317–339.
[5] Yang, R. Y., Zou, R. P., and Yu, A. B., 2003, "Effect of Material Properties on the Packing of Fine Particles," J. Appl. Phys., **94**(5), pp. 3025–3034.
[6] Yang, R. Y., Zou, R. P., and Yu, A. B., 2000, "Computer Simulation of the Packing of Fine Particles," Phys. Rev. E, **62**(3B), pp. 3900–3908.
[7] Landry, J. W., Grest, G. S., and Plimpton, S. J., 2004, "Discrete Element Simulations of Stress Distributions in Silos: Crossover From Two to Three Dimensions," Powder Technol., **139**(3), pp. 233–239.
[8] Sykut, J., Molenda, M., and Horabik, J., 2008, "DEM Simulation of the Packing Structure and Wall Load in a 2-Dimensional Silo," Granular Matter, **10**, pp. 273–278.
[9] Gan, M., Gopinathan, N., Jia, X., and Williams, R. A., 2004, "Predicting Packing Characteristics of Particles of Arbitrary Shapes," Kona, **22**, pp. 82–93. Available at http://www.kona.or.jp/search/22_082.pdf
[10] Shi, Y., and Zhang, Y., 2008, "Simulation of Random Packing of Spherical Particles With Different Size Distributions," Appl. Phys. A, **92**, pp. 621–626.
[11] Zhou, J., Zhang, Y., and Chen, J. K., 2009, "Numerical Simulation of Random Packing of Spherical Particles for Powder-Based Addictive Manufacturing," ASME J. Manuf. Sci. Eng., **131**, p. 031004.
[12] He, D., and Ekere, N. N., 1998, "Computer Simulation of Powder Compaction of Spherical Particles," J. Mater. Sci. Lett., **17**, pp. 1723–1725.
[13] Visscher, W. M., and Bolsterli, M., 1972, "Random Packing of Equal and Unequal Spheres in Two and Three Dimensions," Nature **329**, pp. 504–507.
[14] Anishchik, S. V., and Medvedev, N. N., 1995, "Three-Dimensional Apollonian Packing as a Model for Dense Granular Systems," Phys. Rev. Lett., **75**, pp. 4314–4317.
[15] Scoppe, W., 1990, "Computer Simulation of Random Packings of Hard Spheres," Powder Technol., **62**, pp. 189–196.
[16] Tory, E. M., Church, B. H., Tam, M. K., and Ratner, M., 1973, "Simulated Random Packing of Equal Spheres," Can. J. Chem. Eng., **51**, pp. 484–493.
[17] Jodrey, W. S., and Tory, E. M., 1979, "Simulation of Random Packing of Spheres," Simulation, **32**, pp. 1–12.
[18] Cheng, Y. F., Guo, S. J., and Lai, H. Y., 2000, "Dynamic Simulation of Random Packing of Spherical Particles," Powder Technol., **107**, pp. 123–130.
[19] Leonardo, E. S., Deniz, E., Gary, S. G., Thomas, C. H., and Dov, L., 2002, "Geometry of Frictionless and Frictional Sphere Packings," Phys. Rev. E, **65**, p. 031304.
[20] Mao, K., Wang, M., Xu, Z., and Chen, T., 2004, "DEM Simulation of Particle Damping," Powder Technol., **142**, pp. 154–165.
[21] Jia, T., Zhang, Y., and Chen, J. K., 2011, "Dynamic Simulation of Particles Packing With Different Size Distributions," ASME J. Manuf. Sci. Eng., **133**(2), p. 021011.
[22] Jia, T., Zhang, Y., and Chen, J. K., 2012, "Simulation of Granular Packing of Particles With Different Size Distributions," Comput. Mater. Sci., **51**(1), pp. 172–180.
[23] Jia, T., Zhang, Y., Chen, J. K., and He, Y. L., 2012, "Dynamic Simulation of Granular Packing of Fine Cohesive Particles With Different Size Distributions," Powder Technol., **218**, pp. 76–85.
[24] Alvo, S., Lambert, P., Gauthier, M., and Régnier, S., 2010, "A van der Waals Force-Based Adhesion Model for Micro Manipulation," J. Adhes. Sci. Technol., **24**, pp. 2415–2428.
[25] Santamarina, J. C., 2001, "Soil Behavior and Soft Ground Construction," Proceedings of Symposium Soil Behavior and Soft Ground Construction in Honor of Charles C. Ladd, Oct. 2001, MIT.
[26] Feddema, J. T., Xavier, P., and Brown, R., 1999, "Micro-Assembly Planning With van der Waals Force," Proceedings of IEEE International Symposium Assembly Task Planning, pp. 32–38.
[27] Zhou, Q., Kallio, P., Arai, F., Fukuda, T., and Koivo, H. N., 1999, "A Model for Operating Spherical Micro Objects," Proceedings of 1999 International Symposium on Micromechatronics and Human Science, pp. 79–85.
[28] Kloss, C., Goniva, C., Hager, A., Amberger, S., and Pirker, S., 2012, "Models, Algorithms, and Validation for Open Source DEM and CFD-DEM," Prog. Comput. Fluid Dyn., **12**, pp. 140–152.
[29] Plimpton, S., 1995, "Fast Parallel Algorithms for Short-Range Molecular Dynamics," J. Comp. Physiol., **117**, pp. 1–19.
[30] Tibor, G. J., and Fritz, E., 2005, "Three-Dimensional Discrete Element Simulations in Hoppers and Silos," Powder Technol., **158**, pp. 58–68.
[31] Mindlin, R. D., and Deresiewicz, H., 1953, "Elastic Spheres in Contact Under Varying Oblique Forces," J. Appl. Mech., **20**, pp. 327–344.
[32] Vu-Quoc, L., Lesburg, L., and Zhang, X., 2004, "An Accurate Tangential Force-Displacement Model for Granular-Flow Simulations: Contacting Spheres With Plastic Deformation, Force-Driven Formulation," J. Comput. Phys., **196**, pp. 298–326.
[33] Kruggel, E. H., Wirtza, S., and Scherera, V., 2008, "A Study on Tangential Force Laws Applicable to the Discrete Element Method (DEM) for Materials With Viscoelastic or Plastic Behavior," Chem. Eng. Sci., **63**, pp. 1523–1541.
[34] Hamaker, H. C., 1937, "The London—van der Waals Attraction Between Spherical Particles," Physica, **4**, pp. 1058–1072.
[35] Brilliantov, N. V., Spahn, F., Hertzsch, J. M., and Poschel, T., 1996, "Model for Collisions in Granular Gases," Phys. Rev. E, **53**, pp. 5382–5392.
[36] Silbert, L. E., Ertas, D., Grest, G. S., Halsey, T. C., Levine, D., and Plimpton, S. J., 2001, "Granular Flow Down an Inclined Plane: Bagnold Scaling and Rheology," Phys. Rev. E, **64**, p. 051302.
[37] Zhang, H. P., and Makse, H. A., 2005, "Jamming Transition in Emulsions and Granular Materials," Phys. Rev. E, **72**, p. 011301.